ELSEVIER

Deflection of microcantilever by growing vapor bubble

Heon Ju Lee [a], Young Soo Chang [a], Yoon Pyo Lee [a], Kwang-Hun Jeong [b], Ho-Young Kim [b],*

[a] *Thermal/Flow Control Research Center, Korea Institute of Science and Technology, Seoul 139-791, Republic of Korea*
[b] *Department of Mechanical and Aerospace Engineering, Seoul National University, Seoul 151-744, Republic of Korea*

Abstract

This work investigates the mechanics of microcantilever deflection due to growth of a vapor microbubble. We construct a theoretical model to predict the elastic beam deflection due to the capillary pressure developed by the bubble growing between the beam and a substrate. The theory is in good agreement with our experimental results in both macro- and micro-scales. The deflection of a thin-solid structure due to growing bubbles can be used in such micromachines as microactuators, microgenerators and micropumps, which are operated as immersed in liquid.
© 2007 Elsevier B.V. All rights reserved.

Keywords: Microcantilever; Bubble; Surface tension; Elastocapillarity

1. Introduction

Development of MEMS (MicroElectroMechanical Systems) technology has realized various microactuation techniques using electrostatics [1], piezoelectricity [2], bimetals [3], shape memory effects [4], etc. Among these actuation technologies, actuation of solid structures using microbubbles is of a particular interest because it can be used when moving parts are fully immersed in liquid. Lin et al. [5] deflected a microcantilever beam with a thermal bubble generated by a microheater. Bergstrom et al. [6] vaporized liquid in a cavity to increase the interior pressure and thus to deflect the cavity wall. Based on the similar principle, Xu et al. [7] proposed a micro power generator in which piezoelectric membrane was deflected by vaporization of liquid contained in a cavity. In addition to thermal bubbles, bubbles generated by electrolysis [8] have been used in microfluidic devices, including actuators of a microvalve [9] and a biological cell sorting switch [10].

In those applications relying on the interaction of microbeam or membrane with microbubbles generated either thermally or electrochemically, understanding the mechanics of solid deflection due to bubble is essential for design of devices and evaluation of their performance. Therefore, the aim of this work is to provide a theoretical explanation on the deflection of micro-

cantilever beam due to growing microbubble. The deflection is driven by the capillary pressure inside the bubble that is higher than the surrounding liquid, being an interesting example of "elastocapillary" interactions. The deflection of a thin-solid structure due to capillary force was addressed by Kim and Mahadevan [11] in the context of the surface-tension-driven vertical rise of a liquid between two long hydrophilic sheets, i.e. modified Jurin's problem [12]. In this case, the pressure inside the liquid is lower than the atmospheric pressure, thus the sheets are bent inward to squeeze the liquid into the gap between them. However, for the current problem considered in this work, the bubble pressure is higher than the surrounding pressure and the solid structure is pushed away from the bubble. In the following, we construct a model for the elastic response of the cantilever beam due to the pressure of microbubble determined by the surface tension and the contact angle. To verify the modeling, we perform experiments to measure the deflection of a cantilever using a thermal bubble and compare the results with the theory.

2. Theory of beam deflection

We consider a thin-solid beam that consists of a narrow arm and a wide end plate, as shown in Fig. 1. It is clamped at one end and the other end, i.e. the end plate, interacts with the bubble thus has a large area. Fig. 2 shows the recorded images of a thermal bubble deflecting a cantilever beam. Upon the bubble touching the beam, its contact area with the solid increases accompanying

* Corresponding author. Tel.: +82 2 880 9286; fax: +82 2 880 9287.
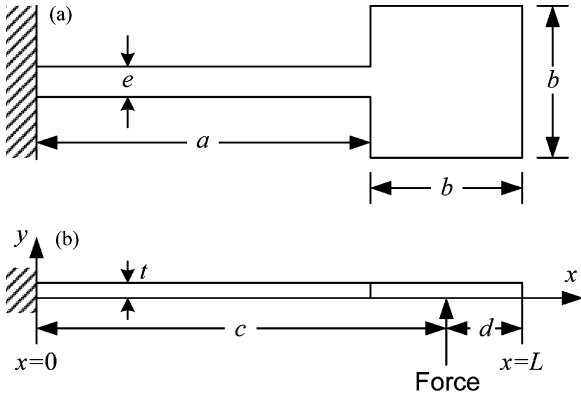 *E-mail address:* hyk@snu.ac.kr (H.-Y. Kim).

Fig. 1. Shape and dimension of a cantilever beam. (a) Top view. (b) Side view.

upward deflection of the beam. The deflection continues until the bubble finally escapes into unbounded region. As the bubble disappears, the beam springs back to an original position and meets a newly formed bubble. Therefore, the deflection process is repeated at a constant frequency. Our focus here is to predict the amount of beam deflection as a function of bubble size and the initial distance between the substrate and the beam.

Rigorously, the end-plate experiences distributed force by pressure difference between inside and outside of the bubble. However, we simplify the load as concentrated force F acting at a point, $x = c$, in the end plate. Assuming a small deflection compared with the length, we use a linear theory of elasticity to describe the deformation of the cantilever. Then the shape of the cantilever $y(x)$ satisfies [13]

$$\frac{d^2}{dx^2}\left(EI\frac{d^2 y}{dx^2}\right) = F\langle x - c\rangle_{-1}, \qquad (1)$$

where E is the solid's modulus of elasticity, $I(x)$ the second moment of area of the beam, c the location of the point load,
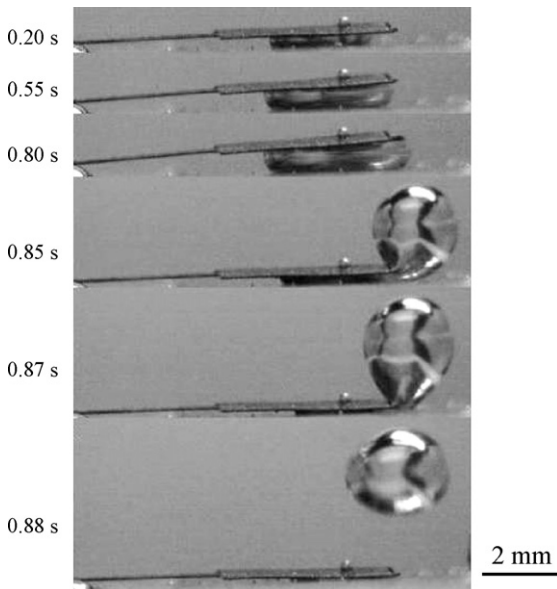

Fig. 2. Sequential images of a growing vapor bubble and a deforming cantilever beam.

and $\langle\cdot\rangle_{-1}$ is the unit impulse function. Integrating Eq. (1) four times gives the cantilever deflection $y(x)$. The beam is clamped at the end $x = 0$ so that $y(0) = 0$ and $y'(0) = 0$. At the other end, $x = L$, we assume no bending moment and shear force, thus $y''(0) = y'''(0) = 0$. These four boundary conditions must be supplemented by matching conditions at $x = a$ given by the continuity of the deflection and the slope: $y(a - \varepsilon) = y(a + \varepsilon)$ and $y'(a - \varepsilon) = y'(a + \varepsilon)$ as $\varepsilon \to 0$. Finally using the global force and torque balances, we can obtain the closed-form expression for $y(x)$:

$$y = \frac{F}{EI_1}\left(-\frac{x^3}{6} + \frac{c}{2}x^2\right), \qquad \text{for } 0 < x < a$$

$$y = \frac{F}{EI_2}\left[\frac{1}{6}\langle c - x\rangle^3 + A(L - x) + B\right], \qquad \text{for } a < x < L$$

where I_1 and I_2 are the second moments of area of the arm and the end plate, respectively $\langle c - x\rangle^3 = 0$ for $x > c$ and $\langle c - x\rangle^3 = (c - x)^3$ for $x < c$. The coefficients A and B are given by

$$A = \frac{I_2}{I_1}a\left(\frac{a}{2} - c\right) - \frac{1}{2}(b - d)^2,$$

$$B = \frac{I_2}{I_1}a\left(\frac{ac}{2} - \frac{a^2}{6} - \frac{ab}{2} + bc\right) + (b - d)^2\left(\frac{d}{6} + \frac{b}{3}\right),$$

where the lengths a, b, c and d are as indicated in Fig. 1. The tip deflection at the free end $x = L$ is $\delta_L = FB/EI_2$. The deflection δ_c at the point where the load is applied, $x = c$, is given by

$$\delta_c = \frac{F(Ad + B)}{EI_2}. \qquad (2)$$

In a case the force acts at the center of the end plate, $c = b/2$, δ_c becomes identical to the result of Ref. [5].

Now we assume that the cantilever velocity is low enough for its inertial and drag force to be negligible and that the hydrostatic pressure difference between the top and bottom of the bubble is much smaller than the capillary pressure. Then the deflection force of the cantilever and the force due to interior pressure of the bubble are balanced to yield $F = \Delta P\pi R^2$, where ΔP is the pressure difference across the bubble interface and R is the contact radius of the bubble and the plate. Fig. 3 shows the schematic of the deflecting beam due to a growing bubble. By
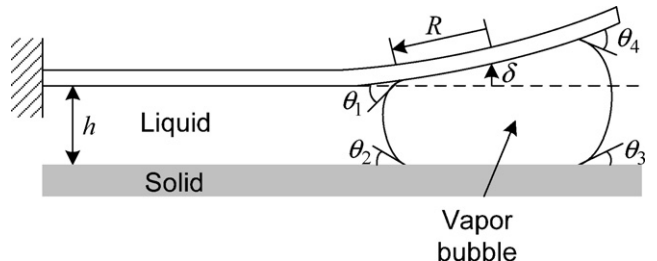

Fig. 3. A schematic of the deflected beam due to a growing bubble.

the Young–Laplace equation, we write

$$\Delta P = \sigma \left(\frac{1}{r} + \frac{1}{R} \right), \qquad (3)$$

where σ is the surface tension and r is the average curvature of bubble meniscus as shown from the side, which will be mathematically defined later in Eq. (5). The local curvature of bubble meniscus near the contact lines as shown from the side, $1/r_i$, is determined by the contact angle θ_i and the spacing between the substrate and the beam $h + \delta$, where h being the distance between the substrate and the clamped end prior to deflection and δ is the deflection:

$$\frac{1}{r_i} = \frac{2 \cos \theta_i}{h + \delta}. \qquad (4)$$

Although δ varies with the location of meniscus, here we simply take $\delta = \delta_c$. The error of r_i due to this simplification is negligible as long as $(\delta_c/h)(b/2a) \ll 1$, that is, when the deflection is small as compared with the clamped height and the end plate is short as compared with the arm. Assuming a general situation where the contact angles at the four corners are not identical, we average the curvature to obtain the average pressure inside the bubble. Therefore, we use

$$\frac{1}{r} = \frac{2s}{h + \delta}, \qquad (5)$$

where s is the averaged cosine of the contact angles, $s = (1/4)\sum_{i=1}^{4} \cos \theta_i$. Combining Eqs. (2) and (3) we can obtain a force balance equation:

$$k\delta = \pi R^2 \sigma \left[\frac{2s}{h + \delta} + \frac{1}{R} \right], \qquad (6)$$

where $k = EI_2/(Ad + B)$. Solving Eq. (6) for δ yields

$$\delta = \tfrac{1}{2}\{(\eta R - h) + [(\eta R - h)^2 + 4\eta R(2Rs + h)]^{1/2}\}, \qquad (7)$$

where $\eta = \pi\sigma/k$. As Eq. (7) indicates, once the material and dimensions of a cantilever, i.e. k, η and h, are given, its deflection is determined by the bubble contact radius R and the contact angles. The equilibrium contact angle values are uniquely given when the solid/gas/liquid combinations are determined. However, for a bubble under compression as considered here, the contact angle values tend to be smaller than the equilibrium values because the contact lines recede. If the evolutions of R and θ_i with time are known, we can explicitly determine the temporal evolution of $\delta(t)$. This involves the consideration of the energy conservation for the bubble's phase change and the dynamics of contact line, both of which fall beyond the scope of the current study.

It is possible to determine theoretically the maximum deflection of a given cantilever using Eq. (7). The bubble cannot grow larger than the end plate, thus the maximum of R is $b/2$. Also assuming that the bubble remains underneath the cantilever until the receding contact angles reach zero, whose validity is to be experimentally examined below, the maximum deflection theo-

retically allowable, Δ_{max}, is

$$\Delta_{max} = \frac{1}{2} \left\{ \left(\frac{\eta b}{2} - h \right) + \left[\left(\frac{\eta b}{2} - h \right)^2 + 2\eta b(b + h) \right]^{1/2} \right\}, \qquad (8)$$

where we put $c = a + b/2$ and $d = b/2$ in evaluating k to get η. If a bubble radius grows only up to $R_{max} < b/2$ before escaping to the unbounded region, the maximum deflection δ_{max} is given by

$$\delta_{max} = \tfrac{1}{2}\{(\eta R_{max} - h)$$
$$+ [(\eta R_{max} - h)^2 + 4\eta R_{max}(2R_{max}s + h)]^{1/2}\}, \qquad (9)$$

where we put $d = R_{max}$. In this section, we have presented the theoretical prediction of the cantilever deflection due to a growing bubble, Eq. (7), and the maximum deflection before the bubble's escape, Eqs. (8) and (9). In the following, we compare our theory with experiments.

3. Experimental results

To verify our theoretical model, we performed a simple experiment to measure the cantilever deflection due to growing thermal bubble. In the experiment, the cantilever was made of 50 μm-thick stainless steel with $a = 9.6$ mm and $b = 5.2$ mm. Thermal bubbles were formed using a nichrome heater housed in a Teflon block covered with a silver tape having a 400 μm-diameter hole through which bubbles were released. The liquid used for this experiment was water and contained in a transparent acrylic tank for optical measurement. The bubble growth and consequent beam deflection were observed through the side of the tank via a high-speed CCD camera, giving rise to the time series illustrated in Fig. 2. An image analysis software (Microsoft Photoeditor) was then used to determine the bubble size and beam deflection.

Fig. 4 shows the temporal evolution of the beam deflection and the bubble-beam contact radius. The contact area increases for the initial 0.4 s or so then the bubble reaches the free end of the beam, which limits the growth of the contact area. However, the beam continues to grow even after the contact area stops increasing, implying that the bubble's interior pressure increases owing to the decrease of the radius r or the contact angles. After the maximum beam deflection is achieved at about 0.8 s, the bubble escapes, leading to the rapid spring-back of the beam.

Fig. 5 compares the theoretical estimation of the beam, Eq. (7), with the beam deflection as the bubble-beam contact radius is given. We used various average cosine values of the contact angles, to find that when $s = \cos 60°$ is used, the theory matches the experimental results until the bubble touches the free end of the beam (from 0 to 0.4 s). Considering that the static contact angles of water with the substrate (silver tape) and the beam were measured in this work to be, respectively, 40° and 83°, it turns out that the average contact angle of the two values result in fairly good agreement between theory and experiment. After the bubble touches the beam free end, the contact angle should decrease following the increase of the bubble curvature. Therefore, from $t = 0.4$ to 0.8 s, the theory matches the exper-
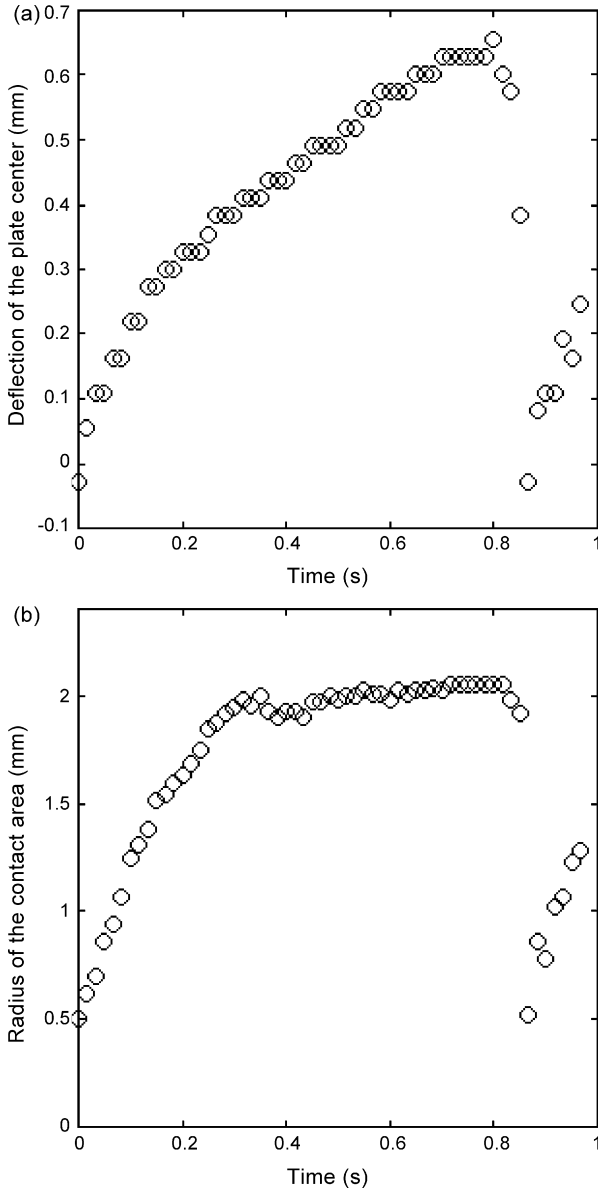
Fig. 4. Measurement results for the temporal evolution of (a) the deflection of the plate center and (b) the radius of the bubble/plate contact area.
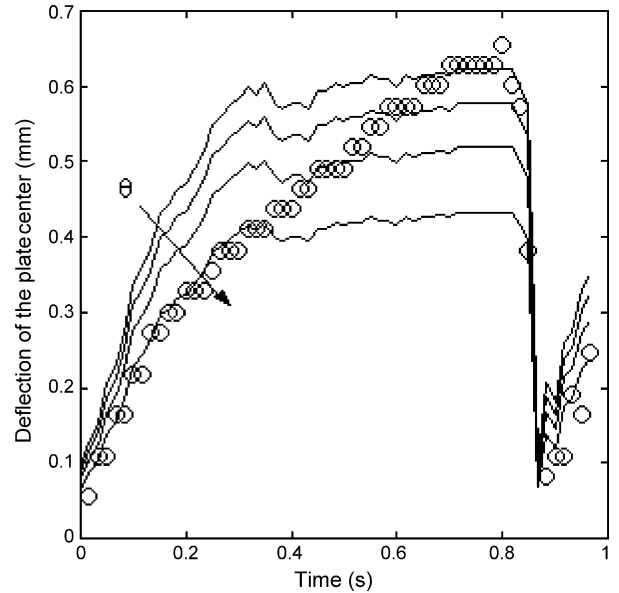

Fig. 5. Comparison of the experimental results (circles) with the theoretical predictions (solid lines). For theoretical predictions, we used different values of θ, and θ increases in the direction of the arrow taking the values 0°, 30°, 45°, and 60°.

tuation system affect the maximum deflection achievable. Fig. 6 shows the effects of the end-plate size, b, the beam thickness, t, and the liquid surface tension on the maximum deflection Δ_{max} of a single-crystal silicon beam. We used Eq. (8) to calculate the maximum beam deflection. As working liquids, we selected water ($\sigma = 0.072$ N/m) and an insulating liquid FC-72 ($\sigma = 0.012$ N/m). Our calculation results show that the beam deflection sensitively increases as the end-plate size increases
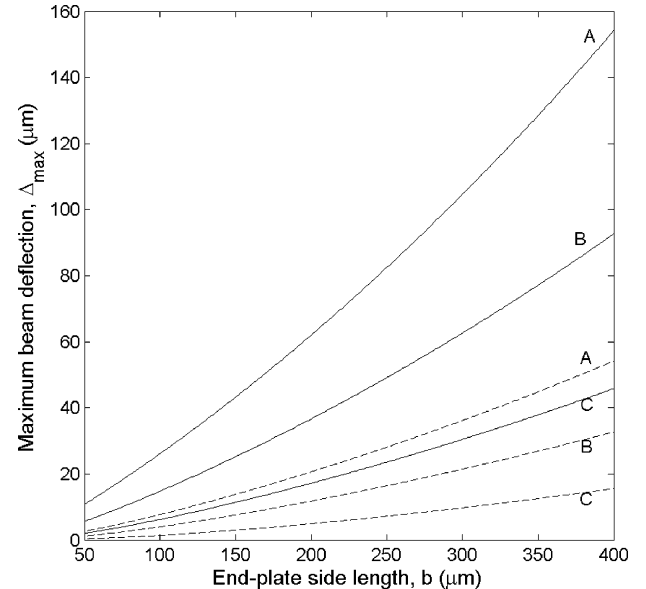
iment when gradually smaller values of θ are used. We find that the maximum deflection is achieved when the contact angle becomes zero ($t = 0.8$ s), validating the foregoing assumption leading to Eq. (8).

To further verify our theory, we fabricated various dimensions of silicon ($E = 190$ GPa) microcantilevers using the bulk micromachining technology [14] and measured their maximum deflection due to growing thermal bubbles formed on platinum microheaters. For the measurement, we used the same optical technique as explained above. Table 1 compares the experimental results and theoretical predictions of each beam's maximum deflection corresponding to the measured maximum radius of the bubble-beam contact area. It shows excellent agreement between the theory and the microscale experiments.

Upon validating our model, it is now possible to investigate how the physical properties and the dimensions of the microac-

Fig. 6. Effects of the beam dimensions and liquid surface tension on the maximum beam deflection possible, Δ_{max}. The solid lines and broken lines correspond to the calculation results using water and FC-72 as working liquids, respectively. The line labels A, B, and C designate the beam thickness of 7.5, 10, and 15 μm, respectively, for each liquid. The arm length a, the arm width e and the initial beam height h were fixed at 800, 50, and 10 μm, respectively.

Table 1
Comparison of the theory and experiments for maximum beam deflections of microscale silicon beams

Exp. No.	t	a	b	e	h	R_{max}	Theoretical δ_{max}	Measured δ_{max}
1	10.3	4040	960	260	199	389	203	195
2	16.5	4040	960	260	233	294	40	42
3	14.4	3040	960	260	222	342	38	38
4	14.4	3040	460	260	223	215	15	14
5	16.5	2040	960	260	214	480	18	18

All the dimensions are in micrometers.

because it increases both the pressure-acting area and the length of moment arm. The decrease of the beam thickness increases the deflection since it decreases the second moment of area. Using a liquid with a high surface tension increases the beam deflection owing to an increased pressure difference given by the Young–Laplace equation. Although not shown here, the effect of the gap height h on the maximum deflection is relatively weak since it determines the bubble radius together with δ.

We finally note that the deflection of the beam should be limited so that the maximum stress occurring at the clamped end does not exceed the yield stress. For a thin beam, the bending stress, τ_b, is dominant over the shear stress and it is given by $\tau_b = 6Fc/et^2$. In the case of a silicon beam of Fig. 6, the maximum bending stress reaches 330 MPa, when $t = 7.5$ μm and $b = 400$ μm. This is an order of magnitude smaller than the yield stress of silicon, 7 GPa.

4. Conclusions

In summary, we constructed a theoretical model to predict the cantilever beam deflection due to a bubble growing between the bubble and the substrate. The model considers the positive interior pressure of the bubble using the Young–Laplace equation, and the deflection is calculated by a linear theory of elasticity. The theoretical predictions are shown to agree fairly well with experimental measurements.

This study can be applied to design an optimal microactuation system where cantilever beams are deflected by vapor bubbles. Although this work provides a theory to calculate the beam deflection as a function of the bubble size and to predict the maximum deflection which is determined by the beam geometry, further study can be pursued to address the growth process of the bubble due to external inputs. For example, thermal bubble growth is governed by a microheater power and the electrochemical bubble can be grown by external voltage inputs. The coupling of the bubble formation process with the beam deflection model will enable the control of the beam deflection using the external inputs. In addition to serving such practical applications, this problem provides one interesting example of elastocapillary theory which solves the deformation of the thin-solid structures due to surface tension effects.

Acknowledgment

References

[1] L.S. Fan, Y.C. Tai, R.S. Muller, IC-processed electrostatic micromotors, Sens. Actuators 20 (1989) 41–47.

[2] R.M. Moroney, R.M. White, R.T. Howe, Microtransport induced by ultrasonic Lamb waves, Appl. Phys. Lett. 59 (1991) 774–776.

[3] W.-H. Chu, M. Mehregany, R.L. Mullen, Analysis of tip deflection and force of a bimetallic cantilever microactuator, J. Micromech. Microeng. 3 (1993) 4–7.

[4] K.D. Skobanek, M. Kohl, S. Miyazaki, Stress-optimised shape memory microactuator, Proc. SPIE 2779 (1996) 499–504.

[5] L. Lin, A.P. Pisano, A.P. Lee, Microbubble powered actuator, in: Proceedings of the International Conference on Solid-State Sensors and Actuators, 1991, pp. 1041–1044.

[6] P.L. Bergstrom, J. Ji, Y.-N. Liu, M. Kaviany, K.D. Wise, Thermally driven phase-change microactuation, J. Microelectromech. Syst. 4 (1995) 10–17.

[7] C. Xu, J. Hall, C. Richards, D. Bahr, R. Richards, Design of a mico heat engine, in: Proceedings of IMECE-MEMS, vol. 2, 2000, pp. 261–267.

[8] C. Neagu, H. Jansen, H. Gardeniers, M. Elwenspoek, The electrolysis of water: an actuation principle for MEMS with a big opportunity, Mechatronics 10 (2000) 571–581.

[9] S. Bohm, W. Olthuis, P. Bergveld, A bi-directional electrochemically-driven micro liquid dosing system with integrated sensor/actuator electrodes, in: Proceedings of IEEE Thirteenth Annual International Conference on Micro Electro Mechanical Systems (MEMS 2000), 2000, pp. 92–95.

[10] C.-T. Ho, R.-Z. Lin, H.-Y. Chang, C.-H. Lin, Micromachined electrochemical T-switches for cell sorting applications, Lab Chip 5 (2005) 1248–1258.

[11] H.-Y. Kim, L. Mahadevan, Capillary rise between elastic sheets, J. Fluid Mech. 548 (2006) 141–150.

[12] J. Jurin, An account of some experiments shown before the Royal Society; with an enquiry into the cause of the ascent and suspension of water in capillary tubes, Philos. Trans. 30 (1718) 739–747.

[13] R.R. Archer, N.H. Cook, S.H. Crandall, N.C. Dahl, T.J. Lardner, F.A. McClintock, E. Rabinowicz, G.S. Reichenbach, An Introduction to the Mechanics of Solids, second ed., McGraw-Hill, Singapore, 1978.

[14] R.C. Jaeger, Introduction to Microelectronic Fabrication, second ed., Prentice Hall, Upper Saddle River, NJ, 2002.

Biographies

Heon Ju Lee received the BS degree from Korea University in 2001 and the MS degree from Texas A&M University in 2003. Now he is a research scientist at Korea Institute of Science and Technology, Seoul, Korea. His research interests are in microscale power generation and fuel cell system controls.

Young Soo Chang received the BS (1991), MS (1993) and PhD (1997) degrees, all from Seoul National University. He is currently a senior research scientist at Korea Institute of Science and Technology, Seoul, Korea. His research interests are in microscale power generation and controls of refrigeration and fuel cell systems.

Yoon Pyo Lee received the BS (1981), MS (1985) and PhD (1989) degrees, all from Seoul National University. He is currently a principal research scientist at

Korea Institute of Science and Technology, Seoul, Korea. His research interests are in sonoluminescence and microscale power generation.

Kwang-Hun Jeong received his BS degree from Busan National University in 2005. He is currently a graduate student in the Micro Fluid Mechanics Laboratory, Seoul National University, Korea. His research interests are in microbubbles and optical tweezers.

Ho-Young Kim received the BS (1994) degree from Seoul National University and the SM (1996) and PhD (1999) degrees from the Massachusetts Institute of Technology, Cambridge, MA, all in mechanical engineering. He is currently an assistant professor in Department of Mechanical and Aerospace Engineering, Seoul National University. His research interest centers around microfluidics and interfacial flow physics.